Supporting Information for

Mapping Allostery through Computational Glycine Scanning and Correlation Analysis of Residue-Residue Contacts

by Quentin R. Johnson, Richard J. Lindsay, Ricky B. Nellas, Elias J. Fernandez, and Tongye Shen

Table S1: 18 residues of the binding pocket of RXR and their interactions with 9C.

Index	Residue	Internal ID	Potential Interactions
1	V265	298	ring, C18
2	C269	302	C18
3	A271	304	COO
4	A272	305	C11, C12
5	Q275	308	COO
6	L309	342	C12
7	I310	343	C9,C18
8	F313	346	C12-COO
9	R316	349	COO
10	A327	360	COO
11	I345	378	C2, ring
12	F346	379	C2, ring
13	V349	382	C16, ring
14	C432	465	C17
15	L433	466	C19
16	H435	468	ring
17	L436	469	C7-C9,C19
18	F439	472	C18

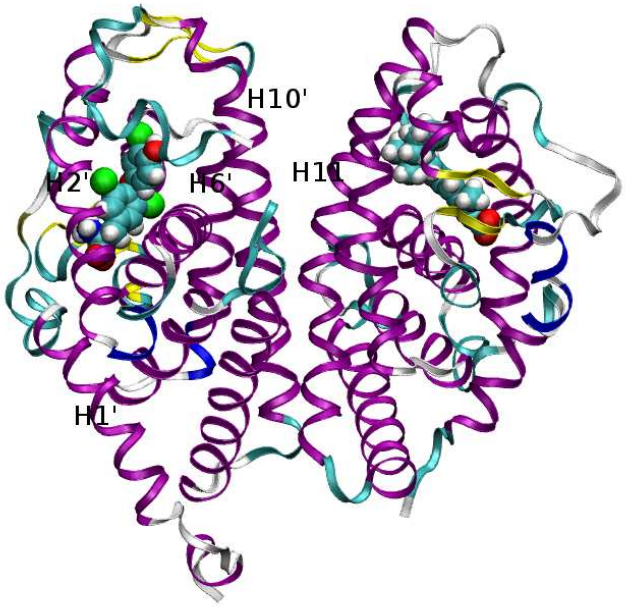

Fig. S 1: A cartoon representation of the TR:RXR complex with important helices labeled.

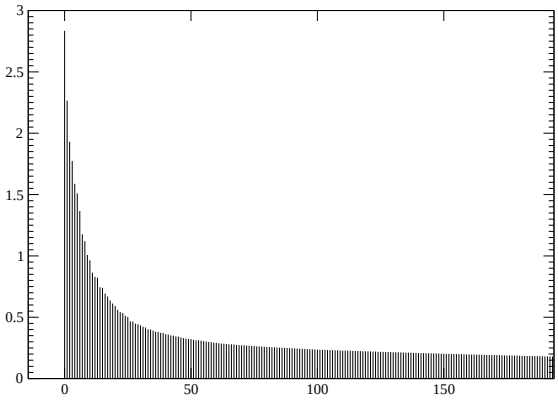

Fig. S 2: The eigenvalues for the diagonalization of the covariance matrix of the contacts. Since the summation of all the eigenvalues is 104.781 (close to 100), the data also closely represents each eigenvalue as the percentage that is normalized by the sum.

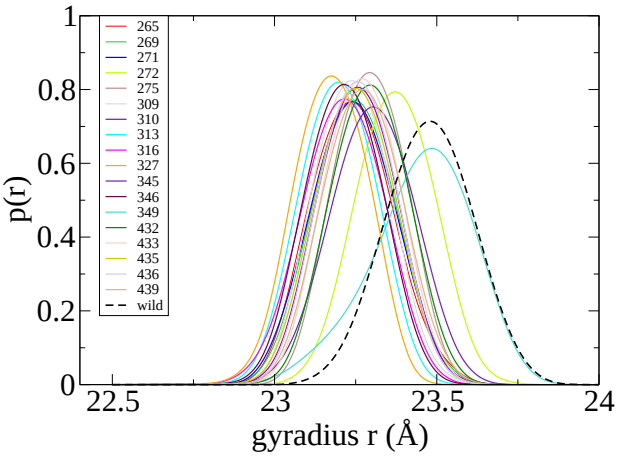

Fig. S 3: The probability distribution of the radius of gyration for each system.

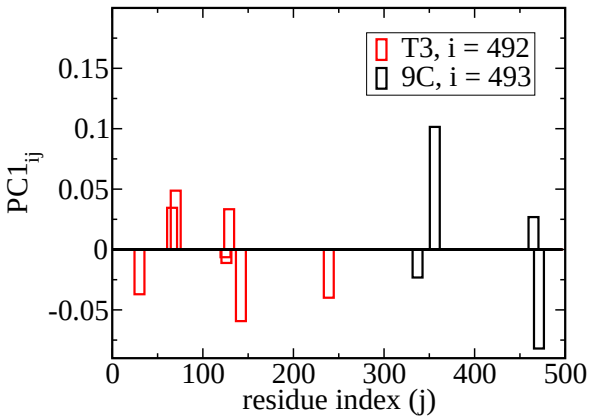

Fig. S 4: The individual components of PC 1 describe the changes of protein-ligand contact formation.

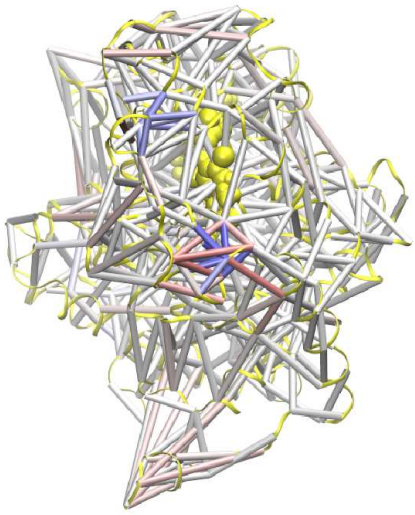

Fig. S 5: A side view (TR side) of PC1 displayed on the 3D cylindrical representation.

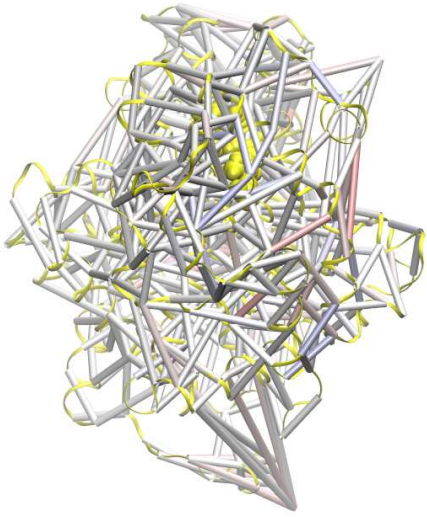

Fig. S 6: A side view (RXR side) of PC1 displayed on the 3D cylindrical representation.

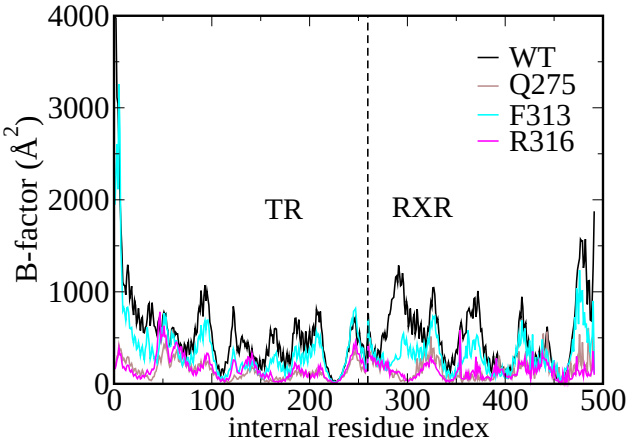

Fig. S 7: The computational B-factor of the protein complex (wild type and selected mutants).

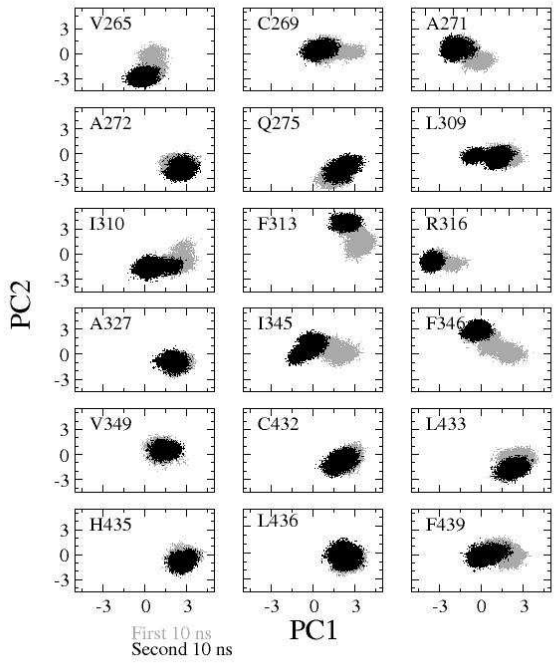

Fig. S 8: To inspect the dynamics, the conformations of the mutants (projected onto PC1 vs PC2) are split into two halves: the first (grey) and second (black) half.